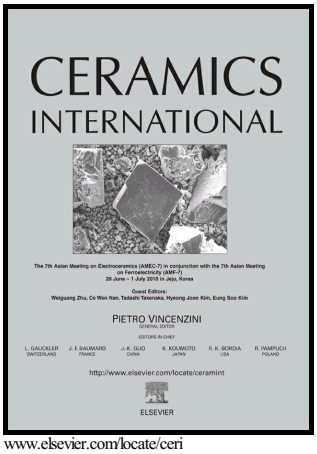

www.elsevier.com/locate/ceri

Damage characterization model of ceramic coating systems based on energy analysis and bending Tests

H.Y. Liu, Y.G. Wei, L.H. Liang, X.H. Liu, Y.B. Wang, H.S. Ma

PII: S0272-8842(17)32763-3
DOI: https://doi.org/10.1016/j.ceramint.2017.12.068
Reference: CERI16948

To appear in: *Ceramics International*

Received date: 9 November 2017
Revised date: 27 November 2017
Accepted date: 9 December 2017

Cite this article as: H.Y. Liu, Y.G. Wei, L.H. Liang, X.H. Liu, Y.B. Wang and H.S. Ma, Damage characterization model of ceramic coating systems based on energy analysis and bending Tests, *Ceramics International,* https://doi.org/10.1016/j.ceramint.2017.12.068

Damage characterization model of ceramic coating systems based on energy analysis and bending Tests

H. Y. Liu[a,b], Y. G. Wei[a,b,*], L. H. Liang[a,c,*], X. H. Liu[a], Y. B. Wang[a], H. S. Ma[a]

[a] *LNM, Institute of Mechanics, Chinese Academy of Sciences, Beijing 100190, China*

[b] *College of Engineering, Peking University, Beijing 100871, China*

[c] *University of Chinese Academy of Sciences, Beijing 101408, China*

ABSTRACT

A quantitative damage model of ceramic coating systems was developed based on their load-displacement curves obtained from three-point bending tests. According to the energy mechanism of damage, the normalized damage rate of such systems can be simply expressed using the load and the tangent slope of their load-displacement curves. The experimental results demonstrated the thickness dependence of fracture and damage. In thin coating systems, tensile failure was found to be predominant and multiple transverse cracks appeared in the coatings. In contrast, thick coating systems showed a predominance of interface shear failure and the occurrence of interface delamination. These observations are consistent with previous experimental results. The damage of the systems displayed catastrophic characteristics when the load tended to reach the failure point, i.e., the damage increased rapidly, and the damage rate displayed a power-law singularity at the failure point. These results are consistent with the damage characteristics predicted using the mathematic model. The damage evolution in the case of interface delamination in the thick coating systems was faster than that for transverse cracking in the thin coatings because of the difference in the degree of damage localization. The present model provides an effective method to elucidate the damage behavior of brittle ceramic coating systems, and hence, it is expected to greatly aid the coating design.

Keywords: ceramic coatings, damage characterization, fracture, thickness effect

* Corresponding authors, *E-mail addresses*: weiyg@pku.edu.cn (Y. G. Wei), lianglh@lnm.imech.ac.cn (L. H. Liang).

1. Introduction

The study of fracture and damage characteristics of ceramic coating systems has gained immense attention because of the wide range of applications of these coatings in many fields. For example, some ceramic coatings are used for the thermal protection of aerospace vehicle engine blades or for corrosion-resistance applications [1–5]. The fracture and spall of ceramic coatings leads to the failure of the alloy substrate parts exposed to high temperatures or corrosion media. Therefore, investigating the intrinsic damage behavior and fracture mechanism of ceramic coating systems is important not only for designing coating parts but also for understanding the damage rule of coating systems. It is well known that bulk ceramic materials show brittle damage and catastrophic failure characteristics. Hao et al. studied the damage of bulk rocks by uniaxial compression experiments and found that a power-law singularity of damage exited at the catastrophic rupture point of the rocks [6]. However, the failure characteristics of ceramic coatings have not been known in detail. An understanding of the failure mechanism of ceramic coatings will be helpful in predicting the failure of important coating parts.

Coating surface cracking and interface cracking between the coatings and the substrates are the main fracture modes observed in the ceramic coating parts exposed to high temperature, thermal shock, or the other extreme conditions [7–14]. This can be attributed to oxidation [7–10], thermal cycles [11–14], thermal-mechanical coupling effects, etc. In order to study the failure mechanism of coating systems, various mechanical loading experiments such as the tensile tests [15–17], four-point bending tests [18–21], three-point bending tests [22–24], etc. were carried out at room temperature [15–24]. These tests are based on the equivalent thermal mechanical energy of ceramic coatings. Zhu et al. carried out a tensile simulation of ceramic coatings and reported that their surface crack density and interface crack length depended on their thickness [15]. In the case of the thin coatings examined in this study, more surface cracks were observed and interface delamination did not occur easily. These results are in the consistence with the four-point bending results reported [19]. Li et al. carried out three-point bending tests on ceramic coating systems and

also reported their thickness-dependent failure [23]. They found that transverse cracks dominated the thin coating systems, while interface delamination was predominated in the thick coating systems. Thouless derived an analytic solution for crack spacing in brittle films on elastic substrates about thirty years ago [25]. McGuigan et al. elucidated the fracture behavior of brittle film/ductile substrate systems with uniaxial tensile strain using an elastic-plastic shear-lag model and calculated their crack density as the function of strain [26]. A delamination–based energy model of segmentation cracking of thin films has also been developed [27]. This model could predict the number of cracks in brittle thin films grown on ductile substrates.

The crack propagation and damage evolution of coating systems have been studied further, and the change rule of the number of transverse cracks in the coatings with strain under mechanical loading has been investigated [16,18, 28–29]. Qian et al. proposed a damage evolution model of coating/substrate/coating sandwich structures under tensile loading [28]. This model included the initiation, propagation, and saturation of transverse cracks in the coatings. Wang et al. investigated the change in the number of microcracks in ceramic coatings with a change in the number of thermal cycles by synchronically observing the microstructure evolution of the coatings under a thermal shock [14]. Schweda et al. investigated the variation of the interface crack area in ceramic coatings with the number of thermal oxidation cycles [30]. Wang et al. studied the evolution of the interface crack area between the ceramic coating and bond layer under a load by carrying out a 3D uniaxial tensile simulation (the tensile direction was vertical to the interface) [31]. Although the microstructure or crack evolution under loading has been observed and fracture modes have been predicted by some models, the development of a quantitative damage evolution model is imperative to predict failure. Recently, an analytic damage model based on the Taylor expansion of controlling stress as the function of damage at the catastrophic failure point has been developed to investigate the crack evolution behavior of the coating systems with different coating thicknesses and microstructures subjected to in–situ three-point bending tests [32]. The power-law relation of damage of all kinds of coatings with controlling stress was found to be same as that of bulk brittle

materials [32]. This model could describe the damage evolution characteristics of ceramic coatings quantitatively. However, this model was based on mathematical derivations and the damage characterization was dependent on the detailed crack evolution. Therefore, a damage model based on mechanical derivations related to physical mechanisms needs to be developed. In previous bending experiments of coating/substrate systems, the slopes of load-displacement curves were found to decrease after the initial linear step [19,23], which corresponded to cracking in the ceramic coatings or interface. The initial nonlinear step (i.e. damage step) needs to be considered since the early damage step is important for complete failure. The use of load-displacement curves to study the damage of ceramic coatings is an attractive idea of characterizing their damage. This method is easy and convenient compared to the detailed capture of crack evolution. Therefore, in this study, a quantitative damage model based on the energy analysis and mechanical derivations was established, and the normalized damage and damage rate with load could be expressed by the change in the tangent slope of the load-displacement curves. In situ three-point bending tests were also performed to obtain real-time load-displacement curves and to verify the model for practical applications.

2. Mechanical damage model

Fig. 1 shows a schematic of load (P)-displacement (w) curve of a ceramic coating system under mechanical loadings (such as tensile or bending loadings). It can be seen from Fig. 1 that at loads higher than the elastic limit load P_e of the system (point E is the turning point from linear to nonlinear response of the curve), the curve deflected and tangent slope of the curve decreased. The tangent slope reduction step is defined as the damage step (EG is the local enlargement of the damage step). The selection of the damage step for the experimental curves will be discussed in section 4. The decrease in the tangent slope of the curve near P_e can be attributed only to the cracking in the coating (or interface). The total potential energy Π of such a system can be written as

$$\Pi = W + U, \tag{1}$$

where W is the external potential energy related to the external force and U is the strain energy. The change in total potential energy because of damage is

$$\left(\Delta\Pi = \Delta W + \Delta U\right)_D = -G_c \Delta D\,, \tag{2}$$

where D is the damage defined by crack area and G_c is the conjugated damage dissipated work in unit area (i.e., the critical energy release rate of cracking). In the

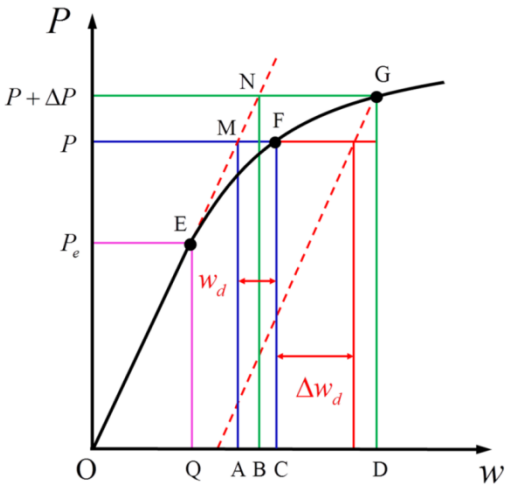

Fig. 1. Mechanical damage model based on the load-displacement curves (sketch map) of ceramic coating systems.

absence of damage, the displacement corresponding to the load P was OA (see point M in Fig. 1). However, in the presence of damage, the actual displacement w was OC (see point F in the load-displacement curve), and the damage displacement w_d was AC, i.e.,

$$w_d = \mathrm{OC} - \mathrm{OA} = w - \frac{P}{k_e}\,, \tag{3}$$

where k_e is the slope of the elastic (linear) step. A small increase in the load (ΔP) resulted in an actual displacement of OD ($w_1 = w + \Delta w$) corresponding to the load $P + \Delta P$ (see point G). In the absence of damage, the displacement should have been OB corresponding to point N. The damage displacement w_{d1} corresponding to $P + \Delta P$ was BD,

$$w_{d1} = \mathrm{OD} - \mathrm{OB} = w_1 - \frac{P + \Delta P}{k_e}. \tag{4}$$

Therefore, the increase in the damage displacement corresponding to ΔP was $\Delta w_d = w_{d1} - w_d$. From Eqs. (3) and (4), we have

$$\Delta w_d = \Delta w - \frac{\Delta P}{k_e}. \tag{5}$$

At the load *P*, the change in external potential energy is given by $\Delta W = -P\Delta w_d$ because of a small increment of the damage displacement, and according to the linear elastic fracture mechanics, $\Delta U = -\frac{1}{2}\Delta W$. By combining these equations with Eq. (2), the following expression can be obtained,

$$\frac{1}{2} P \Delta w_d = G_c \Delta D. \tag{6}$$

If we divide both the sides of Eq. (6) by the corresponding load increment ΔP, the above equation becomes

$$\frac{1}{2} P \frac{\Delta w_d}{\Delta P} = G_c \frac{\Delta D}{\Delta P}. \tag{7}$$

By combining Eqs. (7) and (5) and considering the damage rate to be $R = \frac{\Delta D}{\Delta P}$, the damage rate could be finally obtained from the load-displacement curve as follows,

$$R = \frac{P}{2G_c}\left[\frac{1}{k} - \frac{1}{k_e}\right], \tag{8}$$

where *k* is the tangent slope of the load-displacement curve. Equation (8) shows that the damage rate *R* at any point in the damage step could be obtained by the load *P*, tangent slope *k*, slope k_e of the elastic step, and critical energy release rate G_c.

Furthermore, the integration of both the sides of Eq. (6) yields the damage as $D(w_d) = \frac{1}{2G_c}\int_0^{w_d} P \mathrm{d}w_d$. The combination of this equation with Eq. (5) results in the following relationship: $D(w_d) = \frac{1}{2G_c}\int_{w_e}^{w} P(\mathrm{d}w - \frac{P'(w)}{k_e}\mathrm{d}w)$, where $w_e = \frac{P_e}{k_e}$. Finally, the damage could also be described using the load-displacement curve as follows,

$$D(w_d)=\frac{1}{2G_c}\left[\int_{w_e}^{w} P\mathrm{d}w-\frac{1}{k_e}\int_{P_e}^{P} P\mathrm{d}P\right]=\frac{1}{2G_c}\left[\int_{w_e}^{w} P\mathrm{d}w-\frac{1}{2}(P+P_e)(\frac{P}{k_e}-w_e)\right]. \quad (9)$$

Equation (9) indicates that the damage D corresponding to P was proportional to the difference between the area under the curve EF (S_{EQCF}) and the trapezoid area S_{EQAM}, as shown in Fig. 1. This difference reflects the energy released because of the damage. According to Eq. (9), the damage D could be calculated by fitting the load-displacement curve obtained from the experiments to yield the $P(w)$ function. To verify this damage model for practical applications, in–situ three-point bending tests were carried out on various coating samples. The resulting load-displacement curves were then used to elucidate the damage law.

3. Experimental

3.1. Samples and experimental method

The coating samples used in this study were 8 wt.% Y_2O_3-stabilized ZrO_2 coatings with different thicknesses sprayed on the Ni-based superalloy substrates (GH3128). A Ni-30Cr-12Al-0.3Y bond coating with a thickness of about 10 μm existed between the ceramic top coating and the substrate. For the preparation of the coatings, we used the standard air plasma spray method. The detailed preparation steps can be obtained elsewhere [19,23,33]. The thickness of the substrates h_s was about 1.2 mm. Some of the thick (about 500 μm thick coating) and thin (about 100 μm thick coating) coating systems were used as three-point bending samples with a span length L of 16 mm. The thickness h_c of coatings and the width b of samples are given in Table 1. In order to observe the real-time crack evolution, the in situ three-point bending tests were carried out in the same manner as that used in previous studies [23].

Table 1. Thicknesses of the coatings, widths of the samples, slopes of the elastic steps of the load-displacement curves, elastic limit loads, and failure loads.

Sample symbol	h_c (μm)	b (μm)	k_e(N/mm)	P_e (N)	P_f (N)
S1	100	2630	914	127	223
S2	110	2690	935	124	220
S3	115	2650	924	125	220
S4	485	2640	1076	94	205
S5	500	2620	1086	98	206
S6	480	2610	1063	97	205

The cross-section of the samples was ground and polished. The samples were then placed on the sample platform of an FEI Sirion 400 NC scanning electron microscope (SEM) to carry out in–situ bending tests by the movement of the jig. A mechanical testing apparatus (Gatan Microtest 2000) was used to control this movement. The tests were performed under displacement control. The displacement was measured by a sensor present on the testing apparatus. By applying the displacement load to the substrate surface, the tensile state of the coatings could be achieved, as shown in Fig. 2. The loading rate was 0.1 mm/min. Under the loading condition and through the corresponding load-displacement curves of the coating samples, the real–time crack maps of the coatings, interfaces, and substrates at the cross–section of the samples could be observed by the SEM. To demonstrate the damage evolution, the crack maps were saved by capturing images at a series of loading points. The load-displacement curves were used to elucidate the damage law based on the model.

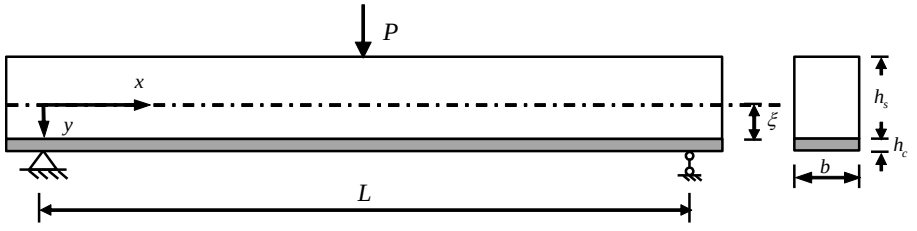

Fig. 2. Schematic of coating (darkened part) samples subjected to the three-point bending tests.

3.2. Experimental results

Fig. 3 shows the load-displacement curves of the coating systems subjected to the three-point bending tests. From the figure, it can be seen that the curves for the coatings with similar thicknesses were almost the same. Note that some small load drops in the curves corresponded to the points at which the images were captured to obtain the real–time crack maps [19,23]. At these points, loading was stopped temporally (resulting in the stress relaxation of the system) and resumed again after capturing the images. However, these stress relaxation did not affect the overall load-displacement curves of the samples. Under the three-point bending condition, at displacements larger than about 0.25 mm, the thick coating systems showed lower loads than the thin coating systems, as shown in Fig. 3. This is mainly because of the interface delamination between the thick coatings and the substrates. Thick coatings lose the ability of bearing load, while thin coatings can bear loading despite their multiple transverse cracking. The parts between the two squares in the curves show the damage steps. The detailed selection of the damage step is discussed in the next section.

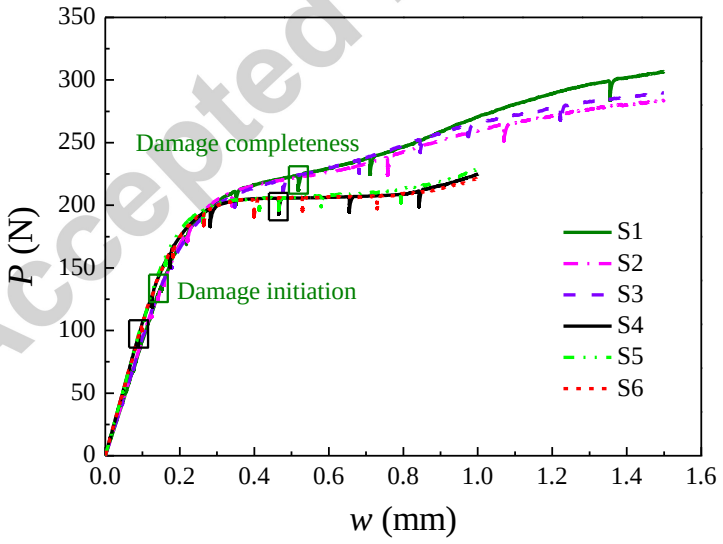

Fig. 3. Load-displacement curves of the thin (S1−S3) and thick (S4−S6) coating systems under the three-point bending tests. The region between the two squares is the damage step.

For a more direct demonstration of damage, the crack evolution maps of the thin

and thick coating systems are shown in Figs. 4 and 5. The corresponding load-displacement curves are shown in Figs. 4(a) and 5(a). It can be seen from Fig. 4(b) that in the thin coatings, the transverse crack evolution included the initiation, multiplication, and saturation steps. In the case of the thick coatings, the interface crack showed faster initiation and progress, as shown in Fig. 5(b). This is in consistence with the previous experimental results [32]. Although in the thick coating systems, a transverse crack appeared before the initiation of interface cracking, the interface shear failure dominated the systems, as was analyzed in a previous study [23]. Thus, for thick coating systems, interface crack evolution is important.

(a)

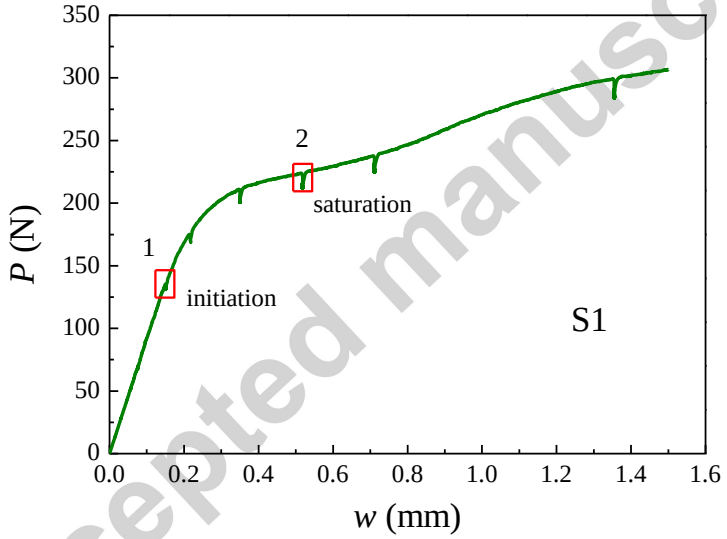

(b)

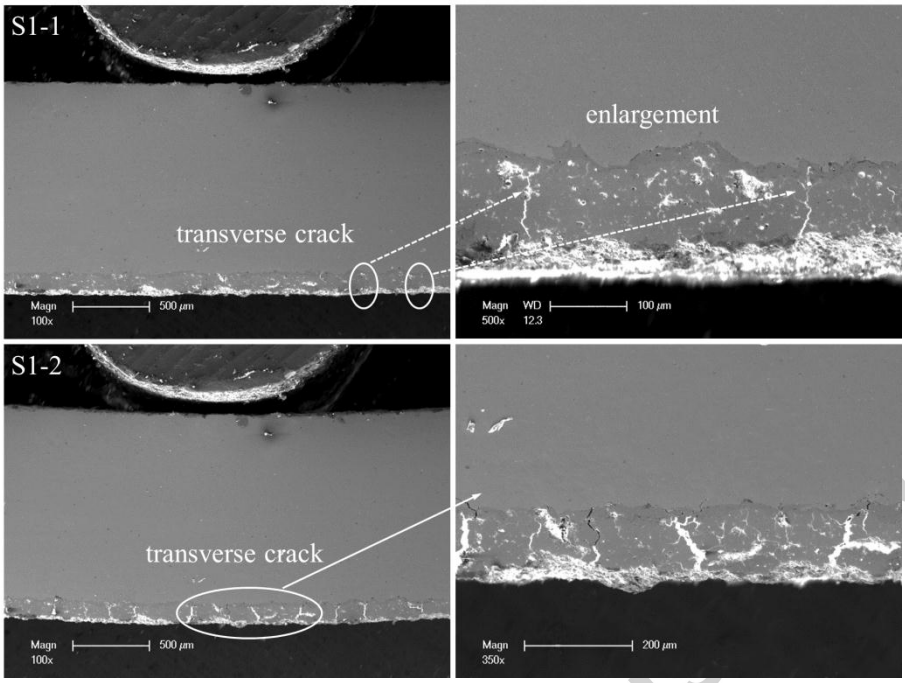

Fig. 4. (a) Load-displacement curve of thin coating system S1, (b) the crack maps corresponding to points 1 and 2 in the damage step of the curve; the right–side maps show the enlargement of some cracks.

(a)

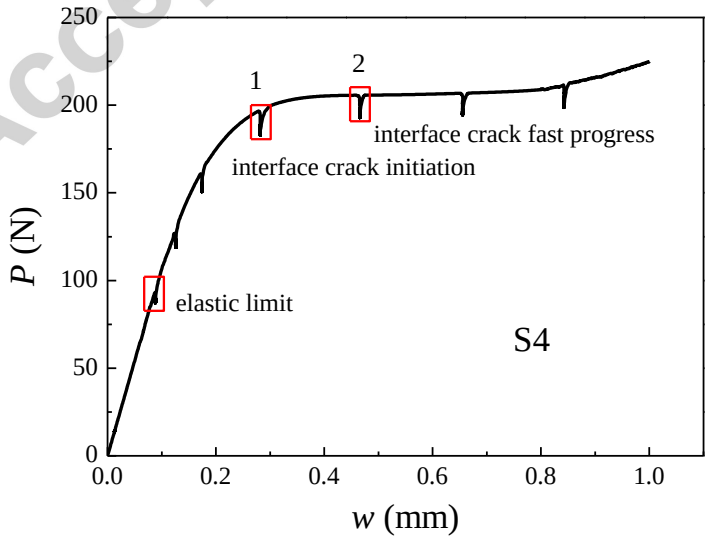

(b)

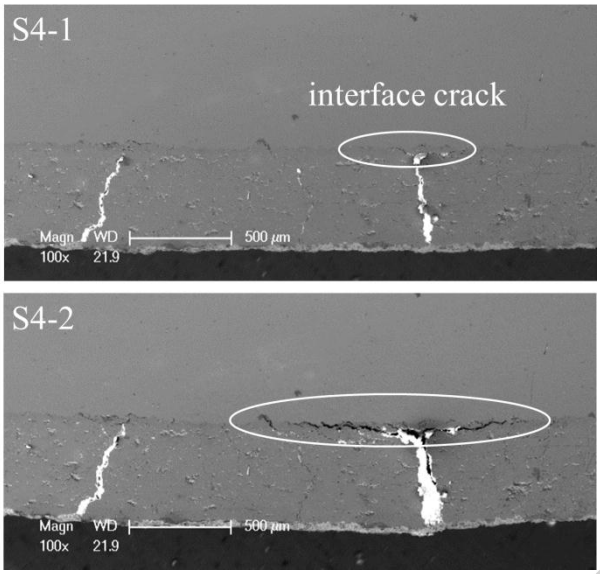

(c)

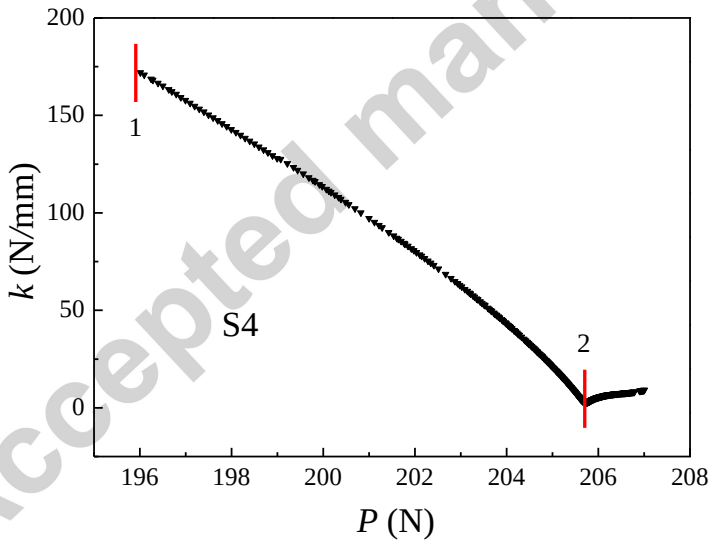

Fig. 5. (a) Load-displacement curve of thick coating system S4, (b) the crack maps corresponding to points 1 and 2 in the damage step of the curve, (c) the corresponding tangent slope changed with an increase in the load, points 1 and 2 correspond to those in (a), respectively.

4. Damage characterization based on the mechanical damage model and experimental results

4.1. Selection of damage step

The load-displacement curves in Fig. 3 were focused on the first two steps i.e.

the linear and damage steps. At small loads, only elastic deformation was observed in the linear step. The damage step is related to the ceramic coating (or interface) cracking. In the damage step, when energy was dissipated by the cracking of the coatings or the delamination of the interface, the stiffness of the systems and the tangent slope of the curves decreased. With a further increase in the load, the plastic deformation of the substrates occurred during the last step and the tangent slope increased again, as shown in Fig. 5(c). Note that plastic substrates do not contribute to the damage step because of their high yield strength (850 MPa [23]) and elastic modulus (200 GPa [23]).

According to the definition of damage, the beginning point of the damage step is the elastic limit of coating systems. At loads higher than the elastic limit load P_e, the coatings showed cracking (Fig. 4 (b)). For thin coating system S1, the end point P_f of the damage step was the point at which the number of transverse cracks saturated, as shown in Fig. 4 (b). This is because the multiple transverse cracking in the coating dominated failure. In thick coating system S4, the damage of the step between the elastic limit and point 1 (Fig. 5 (a)) was caused by transverse cracking in the coating. The interface crack initiated at point 1 (Fig. 5 (b)). The end point P_f of the damage step was the transition point of the change tendency of the tangent slope of the load-displacement curves from decreasing to increasing as shown by point 2 in Fig. 5(c). The interface crack showed a quick progress at the step between the points 1 and 2, and the tangent slope of the curve decreased rapidly. At point 2, an obvious interface crack appeared (Fig. 5 (b)). Considering the fact that the interface shear failure dominated the thick coating systems, only this step of interface damage is shown in Fig. 6 for comparison with the damage in the thin coating systems. The elastic limit load P_e, slope k_e of the elastic step, and failure load P_f are given in Table 1.

4.2. Catastrophic failure behavior

According to the definition of damage rate $R = \frac{\Delta D}{\Delta P}$, in order to compare the

mechanical damage model with a previous normalized mathematic damage model [32], the damage rate can be normalized as

$$R^* = \frac{\Delta D / D_f}{\Delta P / P_f}, \tag{10}$$

where D_f is the crack area at complete damage. By assuming that $\lambda = P/P_f$ and by combining this relation with Eqs. (8) and (9), the normalized damage rate R^* can be written as

$$R^* = \frac{\left[\frac{1}{k} - \frac{1}{k_e}\right] P_f^{\,2}}{\left[\int_{w_e}^{w_f} P\mathrm{d}w - \frac{1}{2}(P_f + P_e)\left(\frac{P_f}{k_e} - w_e\right)\right]} \lambda . \tag{11}$$

Let $D^* = D/D_f$ and combine this relation with Eq. (9), the normalized damage D^* can be written as

$$D^* = \frac{\left[\int_{w_e}^{w} P\mathrm{d}w - \frac{1}{2}(P + P_e)\left(\frac{P}{k_e} - w_e\right)\right]}{\left[\int_{w_e}^{w_f} P\mathrm{d}w - \frac{1}{2}(P_f + P_e)\left(\frac{P_f}{k_e} - w_e\right)\right]}. \tag{12}$$

According to Eq. (11), after the determination of the damage step, the normalized damage rate R^* with an increasing normalized load λ could be obtained using the *k* value of the damage step and k_e. The tangent slope *k* was calculated by fitting the load-displacement curves to obtain the *P*(*w*) functions and solving the differentiation of the functions. Furthermore, according to Eq. (12), the normalized damage D^* with the normalized load λ could be obtained by solving the integral of the *P*(*w*) functions.

Note that the damage law based on Eqs. (11) and (12) is independent of the critical energy release rate G_c. This is because the material parameter G_c is divided out by normalization. Actually, the interface critical energy release rate of the ceramic coating systems varied from 10 to 200 J/m^2 and the reported values show wide variations [34] because of the differences in their microstructure and preparation

conditions. The difference in the methods used to calculate the G_c of thermal barrier coatings is also responsible for these variations. However, the coatings exhibited the same damage law.

Fig. 6 shows the change in the normalized damage rate with an increase in the normalized load during the three-point bending tests. The symbols denote the experimental data (S1-S6) based on the mechanical damage model (Eq. (11)), and the curves were based on a previous mathematical damage model [32]. It can be seen that the damage rate increased rapidly as the load was near the failure point. The damage and failure displayed a catastrophic characteristic, agreeing with the previous studies on the power-law singularity of the damage rate at the failure point [6,32], i.e., $R^* = \frac{C}{2}(1-\lambda)^{-0.5}$ (C is the damage coefficient) [32], the curves in Fig. 6 are the results using the above power-law expression with fitted coefficients from the average experimental data for thin and thick coatings respectively. Fig. 7 shows the change in the normalized damage with an increase in the normalized load during the three-point bending tests. It can be seen that the damage increased obviously as the load approached the failure point. Fig. 6 shows that under the three-point bending conditions, the damage rate R^* of the thick coating systems near the failure point was significantly higher than that of the thin coating systems, indicating that the catastrophic characteristic of the thick coating systems was more obvious. This is because of the difference in the damage localization degrees and failure modes of these coating systems. The damage zone of the interface crack was more localized than that of the multiple transverse cracks. The damage localization has been studied in detail in some previous studies [35–36]. The damage evolution can also be reflected by the controlling variable λ of initial damage (Fig. 7). The damage initiated earlier at the smaller λ for thin coatings (S1–S3), and the initial D^* was also smaller compared to those for interface cracking (S4–S6).

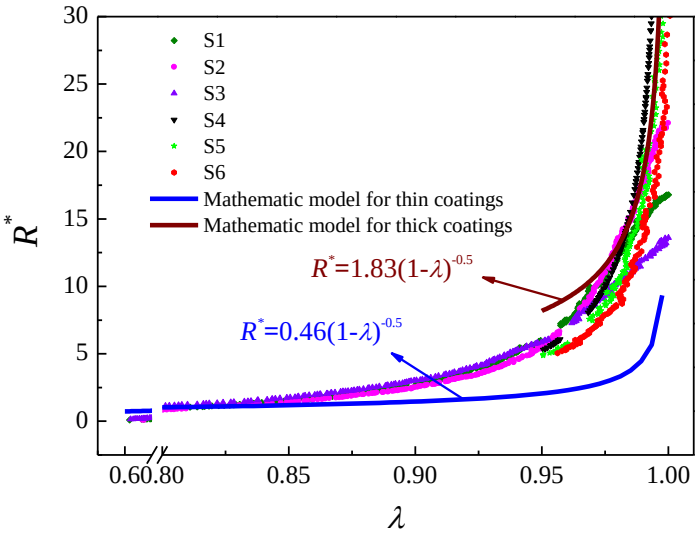

Fig. 6. Normalized damage rate versus normalized load under the three-point bending tests. The experimental results of S1-S6 were based on Eq. (11), two curves were based on the mathematical model [32] as comparisons.

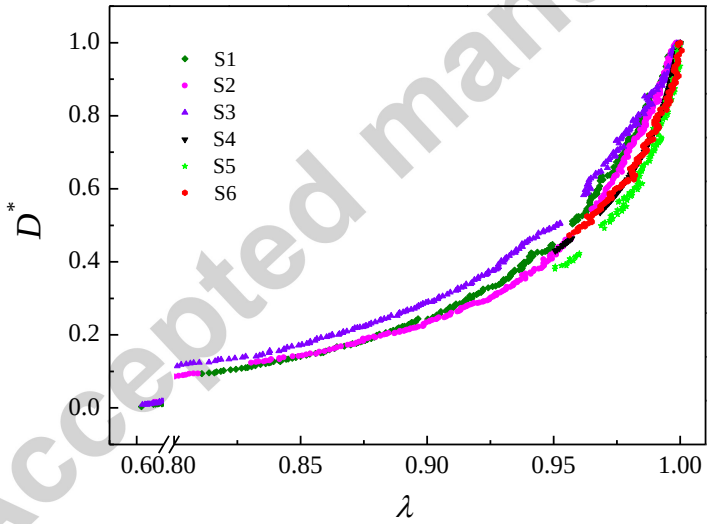

Fig. 7. Normalized damage versus normalized load under the three-point bending tests based on Eq. (12).

In order to verify the model further, the load-displacement curves of the coating systems subjected to the four-point bending tests in Ref. [19] (Fig. 5 in the reference) were also used to characterize the damage rate and damage. In Figs. 8 and 9, S1 and

S4 are the representative samples of the three-point bending tests in present study, and the samples through S7 to S12 are the samples of the four-point bending tests [19]. From Fig. 8, it can be seen that the catastrophic characteristic of the damage under the three-point bending tests was more obvious than that under the four-point bending tests. This is attributed to the higher stress localization degree in the three-point bending samples. The stress in the zone under the three-point bending load was more concentrated, while the stress in the pure bending section under four-point bending was more uniform. Figure 9 also shows that the damage increased obviously up to be complete when the load approached the failure point.

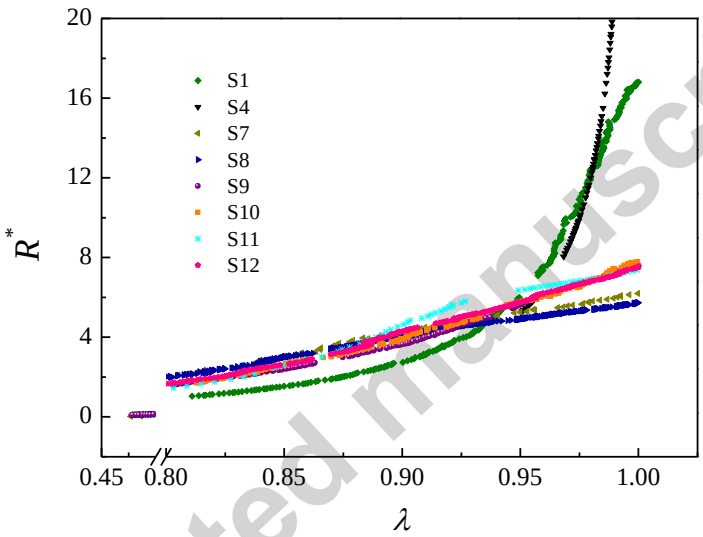

Fig. 8. Comparison of normalized damage rate under the three-point (S1 and S4) and four-point bending (S7 to S12) tests based on Eq. (11).

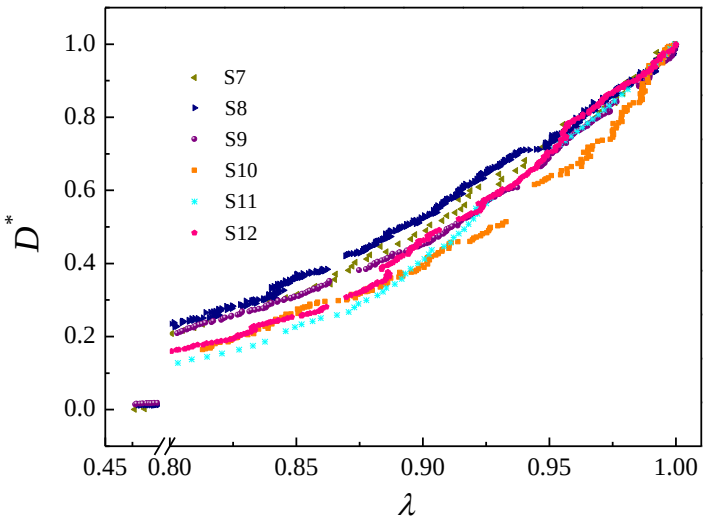

Fig. 9. Normalized damage versus normalized load under the four-point bending tests based on Eq. (12).

Note that microstructures of sprayed ceramic coatings are heterogeneous and experimental data of different samples during same mechanical tests are often scattered, the statistical analysis is usually used to evaluate the failure probability. On the other hand, normalization is an effective method to reveal general rule. Therefore, the normalization of damage was carried out for each sample here, and the experimental results of different samples in terms of Eqs. (11) and (12) showed the same power law (Figs. 6-9) in spite of different absolute values. Damage characterization here reflects the intrinsic law of damage evolution itself from its initiation to completeness despite of different samples or failure modes, and thus, the normalized damage is independent from the critical energy release rate of cracking.

5. Conclusions

In summary, a mechanical damage model for ceramic coating systems was developed based on their load-displacement curves and energy analysis. The corresponding three-point bending experiments of the ceramic coating systems with different coating thicknesses were also carried out. The results show that the model could effectively elucidate the damage and catastrophic failure behavior of the coating systems. The normalized damage, expressed by the change in the tangent slope of the

damage step of the load-displacement curves, increased rapidly with an increase in the load near the failure point. The damage rate showed a power-law singularity at the failure point. The study revealed that the damage rate depended on the damage localization degree. The catastrophic failure characteristic of the thick coating systems dominated by the interface shear failure (an apparent interface crack) under three-point bending was more obvious than that of the thin coating systems, which were dominated by tensile failure (multiple transverse cracks). The model is helpful to understand and predict the damage and failure of ceramic coating systems at room temperature. At higher temperatures, this model should be used with caution because the plastic contribution of substrates increases.

Acknowledgements

This work was supported by the NSFC grants of China (Nos. 11672296, 11372318, 11432014, 11672301), and the Strategic Priority Research Program of the Chinese Academy of Sciences (Grant No. XDB22040501).

References

[1] R. A. Miller, Oxidation-Based Model for Thermal Barrier Coating Life, J. Am. Ceram. Soc. 67 (1984) 517–521.

[2] A. Kobayashi, and T. Kitamura, Effect of heat treatment on high-hardness zirconia coatings formed by gas tunnel type plasma spraying, Vacuum 59 (2000) 194–202.

[3] A. G. Evans, D. R. Mumm, J. W. Hutchinson, G. H. Meier, F. S. Pettit, Mechanisms controlling the durability of thermal barrier coatings, Prog. Mater. Sci. 46 (2001) 505–553.

[4] N. P. Padture, M. Gell, E. H. Jordan, Thermal barrier coatings for gas-turbine engine applications, Science 296 (2002) 280–284.

[5] N. Al. Nasiri, N. Patra, D. D. Jayaseelan, W. E. Lee, Water vapour corrosion of rare earth monosilicates for environmental barrier coatings application, Ceramics International 43 (2017) 7393-7400.

[6] S. W. Hao, F. Rong, M. F. Lu, H. Y. Wang, M. F. Xia, F. J. Ke, Y. L. Bai, Power-law singularity as a possible catastrophe warning observed in rock experiments, Int. J. Rock. Mech. Mining Sci. 60 (2013) 253–262.

[7] S. Ahmadian, C. Thistle, E. H. Jordan, Experimental and Finite Element Study of an Air Plasma Sprayed Thermal Barrier Coating under Fixed Cycle Duration at Various Temperatures, J. Am. Ceram. Soc. 96 (2013) 3210–3217.

[8] N. V. Patel, E. H. Jordan, S. Sridharan, M. Gell, Cyclic furnace testing and life predictions of thermal barrier coating spallation subject to a step change in temperature or in cycle duration, Surf. Coat. Technol. 275 (2015) 384–391.

[9] M. Gupta, R. Eriksson, U. Sand, P. Nylén, A diffusion-based oxide layer growth model using real interface roughness in thermal barrier coatings for lifetime assessment, Surf. Coat. Technol. 271 (2015) 181–191.

[10] T. Beck, R. Herzog, O. Trunova, M. Offermann, R. W. Steinbrech, L. Singheiser, Damage mechanisms and lifetime behavior of plasma-sprayed thermal barrier coating systems for gas turbines –Part II: Modeling, Surf. Coat. Technol. 202 (2008) 5901–5908.

[11] B. Liang, and C. X. Ding, Thermal shock resistances of nanostructured and conventional zirconia coatings deposited by atmospheric plasma spraying, Surf. Coat. Technol. 197 (2005) 185–192.

[12] W. Q. Wang, C. K. Sha, D. Q. Sun, X. Y. Gu, Microstructural feature, thermal shock resistance and isothermal oxidation resistance of nanostructured zirconia coating, Mater. Sci. Eng. A 424 (2006) 1–5.

[13] Z. J. Fan, K. D. Wang, X. Dong, W. Q. Duan, X. S. Mei, W. J. Wang, J. L. Cui, J. Lv, Influence of columnar grain microstructure on thermal shock resistance of laser re-melted ZrO_2-7wt.%Y_2O_3 coatings and their failure mechanism, Surf. Coat. Technol. 277 (2015) 188–196.

[14] Y. Wang, Y. Bai, K. Liu, J. W. Wang, Y. X. Kang, J. R. Li, H. Y. Chen, B. Q. Li, Microstructural evolution of plasma sprayed submicron–/nano–zirconia–based thermal barrier coatings, Appl. Surf. Sci. 363 (2016) 101–112.

[15] W. Zhu, L. Yang, J. W. Guo, Y. C. Zhou, C. Lu, Numerical study on interaction of surface cracking and interfacial delamination in thermal barrier coatings under tension, Appl. Surf. Sci. 315 (2014) 292–298.

[16] M. Zhou, W. B. Yao, X. S. Yang, Z. B. Peng, K. K. Li, C. Y. Dai, W. G. Mao, Y. C. Zhou, C. Lu, In-situ and real-time tests on the damage evolution and fracture of thermal barrier coatings under tension: A coupled acoustic emission and digital image correlation method, Surf. Coat. Technol. 240 (2014) 40–47.

[17] Z. B. Chen, Z. G. Wang, S. J. Zhu, Tensile fracture behavior of thermal barrier coatings on superalloy, Surf. Coat. Technol. 205 (2011) 3931–3938.

[18] Y. C. Zhou, T. Tonomori, A. Yoshida, L. Liu, G. Bignall, T. Hashida, Fracture characteristics of thermal barrier coatings after tensile and bending tests, Surf. Coat. Technol. 157 (2002) 118–127.

[19] H. Y. Liu, L. H. Liang, Y. B. Wang, Y. G. Wei, Fracture Characteristics and Damage Evolution of Coating Systems under Four–point Bending, Int. J. Appl. Ceram. Tec. 13 (2016) 1043–1052.

[20] G. Guidoni, A. Dudekb, S. Patsias, M. Anglada, Fracture behavior of thermal barrier coatings after high temperature exposure in air, Mater. Sci. Eng. A 397 (2005) 209–214.

[21] Y. Zhao, A. Shinmi, X. Zhao, P. J. Withers, S. Van Boxel, N. Markocsan, P. Nylén, P. Xiao, Investigation of interfacial properties of atmospheric plasma sprayed thermal barrier coatings with four-point bending and computed tomography technique, Surf. Coat. Technol.

206 (2012) 4922–4929.

[22] H. X. Deng, H. J. Shi, S. Tsuruoka, Influence of coating thickness and temperature on mechanical properties of steel deposited with Co-based alloy hardfacing coating, Surf. Coat. Technol. 204 (2010) 3927–3934.

[23] X. N. Li, L. H. Liang, J. J. Xie, L. Chen, Y. G. Wei, Thickness-dependent fracture characteristics of ceramic coatings bonded on the alloy substrates, Surf. Coat. Technol. 258 (2014) 1039–1047.

[24] M. J. Tang, H. M. Xie, J. G. Zhu, D. Wu, The failure mechanisms of TBC structure by moire´ interferometry, Mater. Sci. Eng. A 565 (2013) 142–147.

[25] M. D. Thouless, Crack spacing in brittle films on elastic substrates, J. Am. Ceram. Soc. 73 (1990) 2144-2146.

[26] A. P. McGuigan, G. A. D. Briggs, V. M. Burlakov, M. Yanaka, Y. Tsukahara, An elastic–plastic shear lag model for fracture of layered coatings, Thin Solid Films 424 (2003) 219–223.

[27] M. Bialas, Z. Mróz, An energy model of segmentation cracking of thin films, Mech. Mater. 39 (2007) 845-864.

[28] L. H. Qian, S. J. Zhu, Y. Kagawa, T. Kubo, Tensile damage evolution behavior in plasma-sprayed thermal barrier coating system, Surf. Coat. Technol. 173 (2003) 178–184.

[29] W. G. Mao, C. Y. Dai, L. Yang, Y. C. Zhou, Interfacial fracture characteristic and crack propagation of thermal barrier coatings under tensile conditions at elevated temperatures, Int. J. Fract. 151 (2008) 107–120.

[30] M. Schweda, T. Beck, J. Malzbender, L. Singheiser, Damage evolution of a thermal barrier coating system with 3-dimensional periodic interface roughness: Effects of roughness depth, substrate creep strength and pre-oxidation, Surf. Coat. Technol. 276 (2015) 368–373.

[31] L. L. Wang, Q. B. Fan, Y. B. Liu, G. J. Li, H. M. Zhang, Q. S. Wang, F. C. Wang, Simulation of damage and failure processes of thermal barrier coatings subjected to a uniaxial tensile load, Mater. Design 86 (2015) 89–97.

[32] L. H. Liang, X. N. Li, H. Y. Liu, Y. B. Wang, Y. G. Wei, Power-law characteristics of damage and failure of ceramic coating systems under three-point bending, Surf. Coat. Technol. 285 (2016) 113–119.

[33] L. H. Liang, H. Wei, X. N. Li, Y. G. Wei, Size-dependent interface adhesive energy and interface strength of nanostructured systems, Surf. Coat. Technol. 236 (2013) 525-530.

[34] P. F. Zhao, C. A. Sun, X. Y. Zhu, F. L. Shang, C. J. Li, Fracture toughness measurements of plasma sprayed thermal barrier coatings using a modified four-point bending method, Surf. Coat. Technol. 204 (2010) 4066-4074.

[35] Y. L. Bai, J. Bai, H. L. Li, F. J. Ke, M. F. Xia, Damage evolution, localization and failure of solids subjected to impact loading, Int. J. Impact Eng. 24 (2000) 685-701.

[36] S. W. Hao, M. F. Xia, F. J. Ke, Y. L. Bai, Evolution of localized damage zone in heterogeneous media, Int. J. damage Mech. 19 (2010) 787-804.

Captions

Fig. 1. Mechanical damage model based on the load-displacement curves (sketch map) of ceramic coating systems.

Fig. 2. Schematic of coating (darkened part) samples subjected to the three-point bending tests.

Fig. 3. Load-displacement curves of the thin (S1–S3) and thick (S4–S6) coating systems under the three-point bending tests. The region between the two squares is the damage step.

Fig. 4. (a) Load-displacement curve of thin coating system S1, (b) the crack maps corresponding to points 1 and 2 in the damage step of the curve; the right-side maps show the enlargement of some cracks.

Fig. 5. (a) Load-displacement curve of thick coating system S4, (b) the crack maps corresponding to points 1 and 2 in the damage step of the curve, (c) the corresponding tangent slope changed with an increase in the load, points 1 and 2 correspond to those in (a), respectively.

Fig. 6. Normalized damage rate versus normalized load under the three-point bending tests. The experimental results of S1-S6 were based on Eq. (11), two curves were based on the mathematical model [32] as comparisons.

Fig. 7. Normalized damage versus normalized load under the three-point bending tests based on Eq. (12).

Fig. 8. Comparison of normalized damage rate under the three-point (S1 and S4) and four-point bending (S7 to S12) tests based on Eq. (11).

Fig. 9. Normalized damage versus normalized load under the four-point bending tests based on Eq. (12).

Table 1. Thicknesses of the coatings, widths of the samples, slopes of the elastic steps of the load-displacement curves, elastic limit loads, and failure loads.